Hindawi
Journal of Chemistry
Volume 2022, Article ID 8633545, 8 pages
https://doi.org/10.1155/2022/8633545

Research Article

Kinetic Study of the Removal of Methyl Orange Dye by Coupling WO_3/H_2O_2

N'goran Sévérin Eroi, Aimé Serge Ello, Donourou Diabaté, and Konan Roger Koffi

Laboratoire de Constitution et Réaction de La Matière, UFR SSMT, Université Felix Houphouët-Boigny, 22 Bp 582, Abidjan 22, Côte d'Ivoire

Correspondence should be addressed to Aimé Serge Ello; elloserge@gmail.com

Received 11 July 2022; Revised 1 September 2022; Accepted 5 September 2022; Published 24 September 2022

Academic Editor: Ahmad M. Mohammad

In the present work, the heterogeneous Fenton-like process was employed to investigate the kinetic models of the degradation of methyl orange (MO) using tungsten oxide/hydrogen peroxide couple. Tungsten oxide particles were successfully synthesized by reflux without surfactant and characterized by using XRD, SEM, TEM, and FT-IR techniques. The influence of parameters such as temperature and concentration of MO was studied and pseudo first-order and second-order models were applied. WO_3/H_2O_2 showed high efficiency in the removal of methyl orange and attained more than 92.8% in 180 min. The first-order kinetic model was described by the removal process with the correlation coefficient of $R^2 = 0.99$.

1. Introduction

Advanced oxidation processes based on UV, photo catalysis, Fenton, and Fenton-like oxidation were suggested for the removal of pollutants from an aqueous media [1–6]. Among these methods, Fenton reactions attracted much attention and showed high removal efficiency of different dyes from wastewater [7–10]. The classical Fenton reaction using iron salts (Fe^{2+} or Fe^{3+}) and H_2O_2 can produce powerfully oxidizing radical species such $HO^\bullet$ for decomposition of dyes:

$$Fe^{2+} + H_2O_2 \longrightarrow Fe^{3+} + HO^\bullet + OH^-, \quad (1)$$

$$Fe^{3+} + H_2O_2 \longrightarrow Fe^{2+} + HO_2{}^\bullet + H^+. \quad (2)$$

However, the implementation of homogeneous Fenton oxidation based on ferrous or ferric salts has several limitations, including the conversion of Fe $(OH)_3$ into sludge at pH above 4 [11]. To improve the oxidation efficiency, heterogeneous Fenton-like reaction has been developed. Heterogeneous Fenton-like process was established by replacing Fe^{2+} in the Fenton reagent with a solid catalyst including metal oxide. It was shown that metal oxide decomposes hydrogen peroxide H_2O_2 to hydroxyl radical $HO^\bullet$ as in classical Fenton reaction [11–13] and then successfully used as heterogeneous catalysts for degradation of organic pollutants. The following mechanism generating $HO^\bullet$ from H_2O_2 was proposed for Mn_3O_4/H_2O_2 [14] and Cr (VI)/H_2O_2 [15].

$$M(VI)surf + H_2O_2 \longrightarrow M(V)surf + HO^\bullet + HO^-, \quad (3)$$

$$M(V)surf + H_2O_2 \longrightarrow M(VI)surf + HO^\bullet + HO^-. \quad (4)$$

M is a metal oxide and VI and V are the oxidation states, respectively. The reduction of M (VI) on the surface generates radical hydroxyl species (3), and the reactive M (V) species are capable of generating $HO^\bullet$ from H_2O_2 (4). Heterogeneous Fenton-like oxidation process has an advantage over the classical Fenton process. The recovery of catalysts or metal oxides is easily and prevents precipitate of iron hydroxide (sludge) as shown in classical Fenton process [11]. Several works for the green elimination of dyes were investigated with the heterogeneous Fenton-like methods using different metal oxides. Thus, hematite (α-Fe_2O_3) nanostructures and iron oxide supported on carbon

nanotube (Fe_3O_4/MWCNTs) were used as heterogeneous Fenton catalysts and showed 76.6% [16] and 91.9% [17], respectively, to the removal of methyl orange (MO). Iron oxide (Fe_2O_3) coated on the surface of sand showed 60% of methyl orange removal and increased to 74% with heterogeneous photo Fenton system [18]. In the strong acid media, it was possible to oxidise more than 97.8% of methyl orange [19] using Fenton reaction. According to previous work, tungsten oxide used as a heterogeneous Fenton-like catalyst resulted in a good efficiency in the degradation of methyl orange and indigo carmine [20, 21]. However, these works involving this heterogeneous system for the removal of recalcitrant dyes did not elaborate on the kinetic models of their studies. The aim of this project is to investigate kinetic models of the heterogeneous Fenton-like process using WO_3 as a new metal oxide catalyst for the removal of methyl orange, which is an azo dye widely applied in various industries. Additionally, tungsten oxide particles were characterized, and the optimal removal parameters such as temperature and pollutant concentrations were investigated. These methods are very simple and exhibit very high oxidation potential.

2. Materials and Methods

2.1. Preparation of Tungsten Oxide Particles. Tungsten oxide particles were prepared by a simple dispersion of metallic tungsten powder (1 g) (APS 1-5 μm, purity 99.9%, Alfa Aesar Co) in deionized water (10 ml), glacial acetic acid (1 ml, ACS reagent, purity ≥99.7%) followed by addition of H_2O_2 (10 ml, aqueous solution; 30%, Fisher Scientific Co) drop wise. The solution was heated at 358 K for 3 h to form tungsten oxide particles. The tungsten oxide particles were washed with water and then dried at 333 K overnight (16 h) and annealed at 373 K for 4 h.

2.2. Characterization. Powder X-ray diffraction (XRD) patterns of the tungsten oxide particles were obtained on a Bruker D8 Advance X-ray diffractometer equipped with a CuKα radiation source ($\lambda = 1.5418$ Å). Scanning electron microscopy (SEM) image was taken on a JEOL 6360 instrument at an accelerating voltage of 3 kV. Transmission electron microscopy (TEM) images and energy dispersive X-ray spectroscopy (EDS) were taken on a JEOL/JEM-2100F operated at 200 kV. Fourier transform infrared (FT-IR) absorption spectra were measured with an FTS 45 infrared spectrophotometer using KBr pellet technique.

2.3. Fenton-like Experiments. The removal of methyl orange dye was carried out in a reactor capacity of 250 ml previously heated and maintained at various temperatures (303–338 K). The reactor was loaded with 100 ml of various concentrations of MO aqueous solution and 250 mg of tungsten oxide particles under stirring. The heterogeneous Fenton-like degradation process was initiated by adding 2.5 mL of H_2O_2 carefully. The mixture was continuously stirred using a magnetic stirrer, and tungsten metal oxide particles were separated from aqueous solution at the end of the reaction time.

The residual concentration of MO from the aqueous solution was determined via UV-vis spectrophotometer at 464 nm. The rate of removal of MO was obtained by Eq. (5) below.

$$\%\ \text{removal} = \frac{(C_0 - C_t)}{C_0} \times 100\%, \tag{5}$$

where C_0 and C_t are the initial and residual concentrations of MO, respectively.

Based on the MO degradation profile, first-and second-order kinetic models are expressed by Eq. (6-7).

$$\ln \frac{C_0}{C_t} = k_1 t, \tag{6}$$

$$\frac{1}{C_t} - \frac{1}{C_0} = k_2 t, \tag{7}$$

where C_0 is the initial MO concentration, C_t is the MO concentration at various times (t) and temperatures, and k_1 and k_2 are the rate constants for pseudo zero, first-and second-order reactions, respectively, at different temperatures.

3. Results and Discussion

The XRD analysis was applied to identify the structure of tungsten oxide synthesized and we obtained the pattern showed on Figure 1.

The major peaks appeared at $2\theta = 16.53$, 25.63, 35.03, and 49.64 degree were assigned to (020), (111), (131), and (202) planes related to the structure of the hydrated tungsten oxide of orthorhombic structure (JCPDS card N°84-0886) [22, 23]. All the strong and sharp diffraction peaks indicated high degree of crystallization. SEM image of tungsten oxide synthesized reveals nonregular nanoplates in Figure 2(a). TEM image of tungsten oxide is shown in Figure 2(b), and the irregularly shaped particles and near to rectangular particles are in the nanosize.

Figure 2(c) depicts the EDS surface analysis of WO_3 particles. The spectrum showed major peaks corresponding to W (tungsten) and O (oxygen). The element of Cu arises from the use of Cu grids during TEM analysis [24]. The ratio of W to O peak was in proximity of 1 : 3 as expected. Figure 2(d) shows the FT-IR spectrum of tungsten oxide synthesized. The symmetric stretching vibrations (W-OH... H_2O) at 3397 cm^{-1} are attributed to intercalated water [25, 26]. We also observed the bending vibration peak located at 1613 cm^{-1}, which corresponds to the W-OH plane [25, 27] in agreement with the hydrated orthorhombic structure showed with XRD. FT-IR confirmed the presence of water in the sample. The various vibration peaks at 942 and 671 cm^{-1} were assigned as the stretching of W=O and O-W bonds, respectively [25, 28]. According to the results of the XRD pattern, TEM-EDS images, and FT-IR spectrum, hydrated orthorhombic tungsten oxide WO_3-H_2O was successfully synthesized.

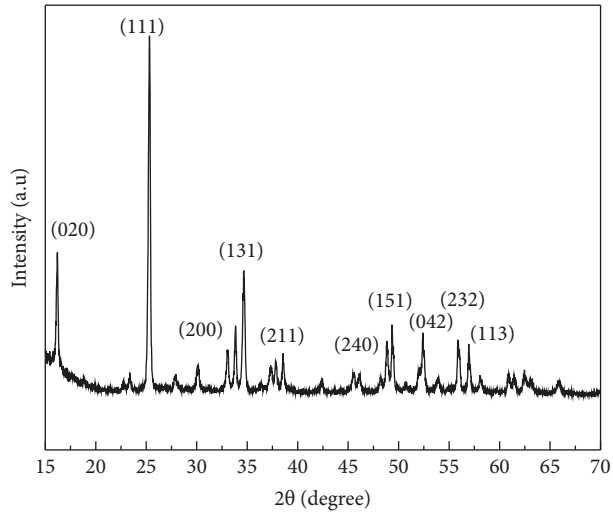

Figure 1: XRD pattern of tungsten oxide synthesized.

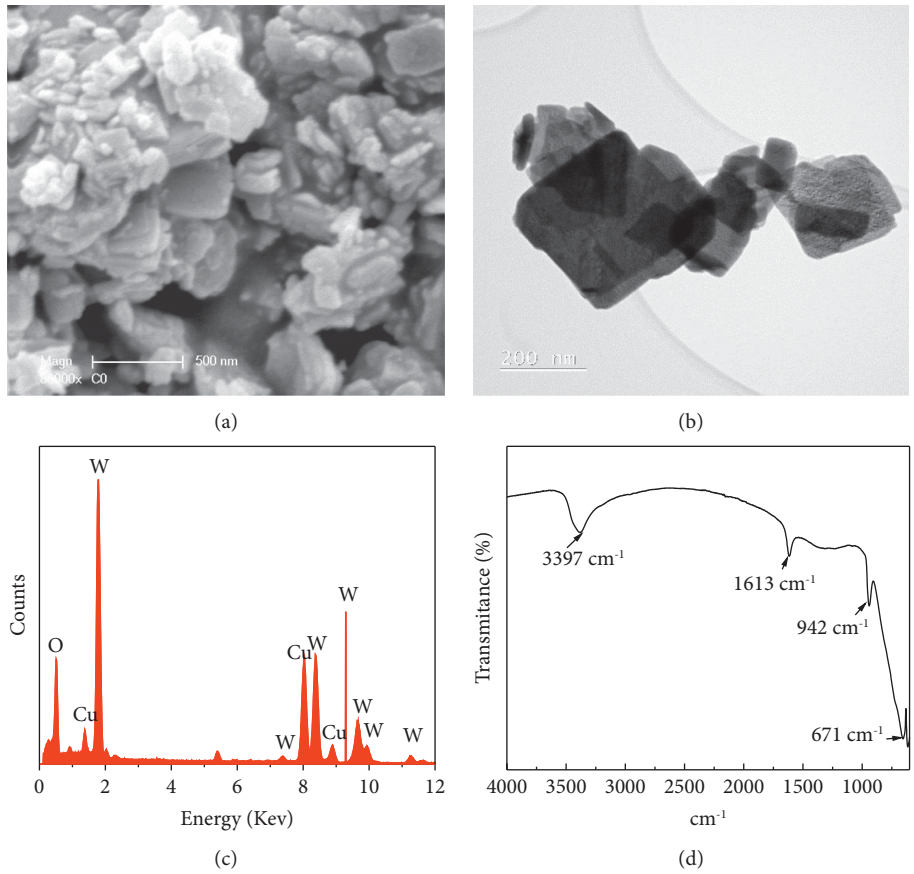

Figure 2: (a) SEM image of tungsten oxide synthesized, (b) TEM image of tungsten oxide synthesized, (c) EDS spectrum of tungsten oxide synthesized, and (d) FT-IR spectrum of tungsten oxide synthesized.

Figure 3 shows that when hydrogen peroxide is only used to remove MO, the removal rate increased to 12.5% at pH 4. This value of pH was previously observed as an optimal condition to remove MO [20]. The removal rate of MO decreased around 3% when WO_3 was as used the catalyst. In fact, hydrogen peroxide has a high oxidation capacity and showed high efficiency of removal of organic dyes [29].

The coupling of WO_3/H_2O_2 considerably increased the rate of removal of methyl orange to 43%. The performance of the WO_3/H_2O_2 couple was much higher than when tungsten oxide and hydrogen peroxide are used alone. According to

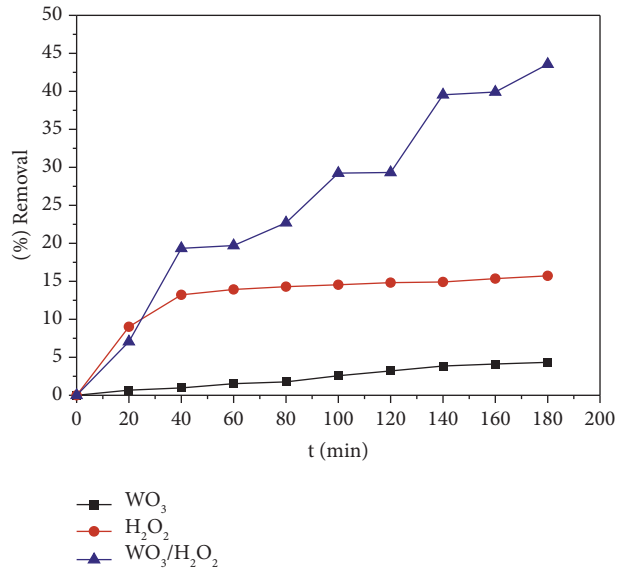

Figure 3: Effect of catalysts on the rate of removal of MO: experimental condition: pH = 4, (OM) = 30 mg L^{-1}, V_{H2O2} = 2.5 ml, T = 303 K mass of WO_3 = 0.25 g.

the literature, tungsten oxide nanoparticles with H_2O_2 can generate reactive oxygen species such as $HO^{\bullet}$ [30] in acidic media [31–33]. The mechanism of MO degradation was studied in our previous works. The degradation of methyl orange with WO_3/H_2O_2 leads to breaking of the azo bond (N=N) following the benzene ring which generates intermediates species. These results are consistent with the works reported in previous literature [18]. The effect of temperature was also studied. The efficiency of the couple WO_3/H_2O_2 was shown in the Figure 4.

The increase of the reaction temperature from 303 to 338 K showed the enhancement of the rate of MO removal (Figure 4(a)). The optimum temperature for the most effective degradation of MO was 338 K, and the efficacy reached 87%. The increase of the performance with temperature is in agreement with the degradation of organic dyes by advanced oxidation processes [34, 35]. The enhancement of the degradation with increasing temperature was also observed in black amido 10B and methylene blue [35, 36].

In fact, the increase of temperature activated more the reaction between H_2O_2 and metal oxide and increased $HO^{\bullet}$ species [35, 38]. The kinetic of MO removal was showed at different temperatures (Figure 4(b)). The pseudo first-order kinetic model fitting the experimental data was significantly affected by reaction temperature (Figure 4(b)). The correlation coefficients were high (R^2 = 0.982, 0.968, 0.993, and 0.997) at 303, 313, 323, and 338 K, respectively. Thus, the results of the experiments indicated that degradation of MO dye by heterogeneous Fenton-like process was better described by the pseudo first-order kinetic model. The result was in agreement with the studies conducted by previous works reported in Table 1 on decolorization of dyes with Fenton process [16, 34, 37]. The pseudo first-order observed in our work was compared with the kinetic parameters of MO removal reported in the literature in Table 1. The results showed a consistency with the literature. The Arrhenius expression is the relationship between the reaction temperature, and the specific reaction rate constant k is expressed as follows:

$$k = \mathrm{A}\exp\left(-\frac{\mathrm{Ea}}{\mathrm{RT}}\right), \tag{8}$$

where A is the pre-exponential factor, E_a is the activation energy (J·mol^{-1}), R is the ideal gas constant (8.314 JRTmol^{-1}·K^{-1}), and T is the reaction absolute temperature (K). The Arrhenius expression showed good linear relationships between the plots of ln (k) and 1/T (Figure 4(c)) because the regression coefficient was higher than 0.997. The calculated activation energy of the degradation reaction of MO was 63.4 J·mol^{-1}. The study of various concentrations of MO was carried out at 338 K and the results are shown in Figure 5(a). We observed the removal efficiency of MO decreased from 92.8% to 76.8% when concentration of MO increased from 15 mg·L^{-1} to 60 mg·L^{-1}, respectively. The increase of initial methyl orange concentrations was opposite to the degradation efficiency previously observed [19, 37]. The decrease of the rate of removal efficiency is due to the relative lower concentration of $HO^{\bullet}$ species resulting from the increasing concentration of MO. The hydroxyl radical ($HO^{\bullet}$) is a nonselective oxidant and can oxidise not only target pollutants but also the intermediates generated during the reaction process. However, the high rate of removal of MO is observed in the concentration of 15 mg·L^{-1}.

Figures 5(a)-5(b) show the fitting plots of first- and second-order models at 338 K. In order to fit the best experimental data, the correlation coefficients of both models were compared. They indicated that the first-order kinetic models fitting of the experimental data showed high values of R^2 as shown in Table 2. First-order kinetic model is more in agreement with the experimental data than the second-

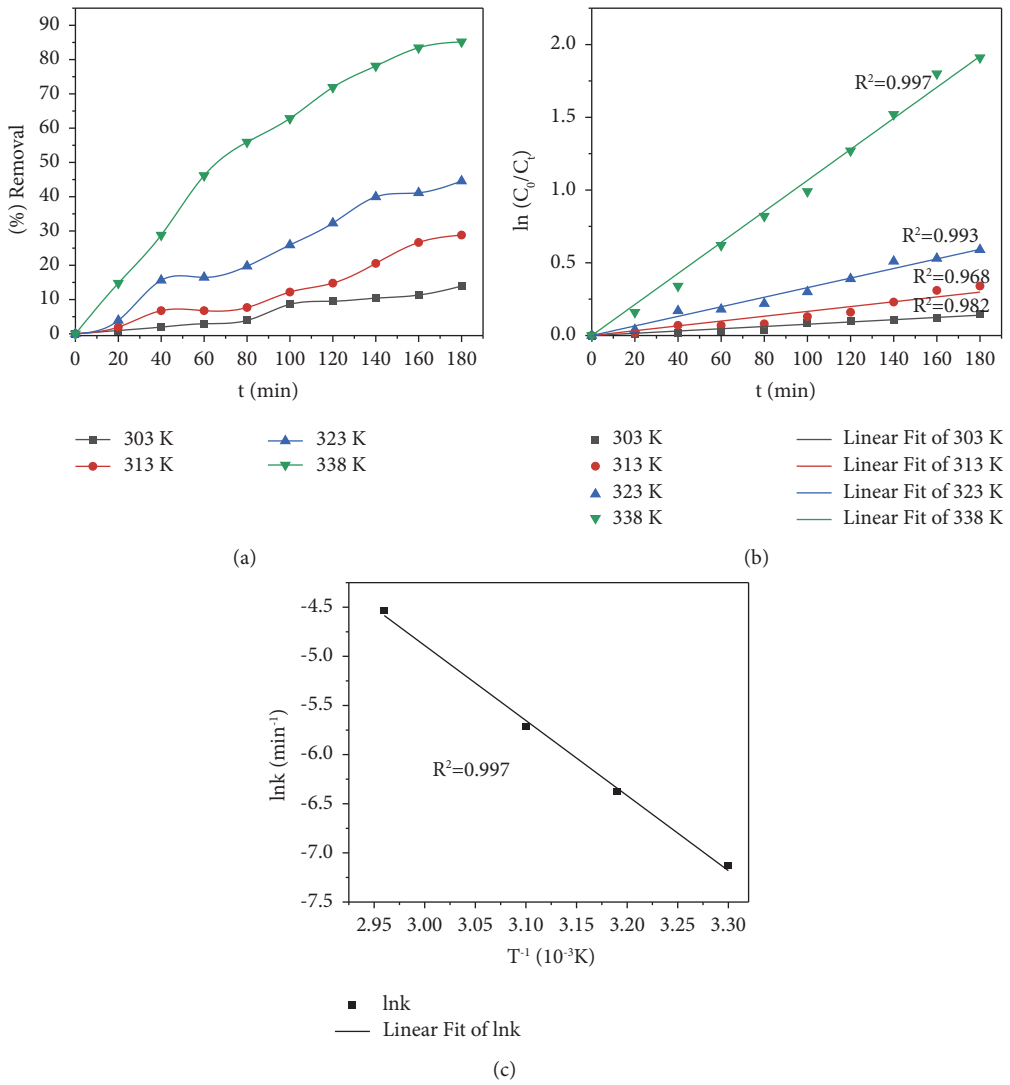

Figure 4: (a) Effect of temperature on the rate of removal of MO. Experimental conditions [MO] = 30 mg. L^{-1}, pH = 4, mass of WO_3 = 0.25 g. (b) Effect of temperature on the first-order kinetic of MO removal. (c) Arrhenius plots of MO degradation.

Table 1: Comparison of the efficiency and kinetic parameters of MO removal.

	(MO)	Catalyst	$[H_2O_2]$	*p*H	Yield	Order	R^2	k (min^{-1})	(Ref.)
Photo-Fenton	30 mg·L^{-1}	Co-SMA 29.92 g L^{-1}	37 mM	4.3	94.79	First order		0.017	[37]
Fenton Fe^{2+}/H_2O_2	5.4×10^{-5}	$(Fe^{2+}) = 1.9 \times 10^{-4}$	2.93×10^{-3}M	2.79	97.8	Second order	0.867	4.9273×10^4 M^{-1}	[19]
Photo-Fenton	2.5 ppm	αFe_2O_3 30 mg	30 μl	—	76.6	First order	0.969	0.0118	[16]
Photo-Fenton	100 mg·L^{-1}	Fe-Sand 1.5 g·L^{-1} Fe-Sand 1.5 g·L^{-1} + UV	200 mg·L^{-1} —	2.5	60 74	—	—	—	[18]
Heterogeneous-Fenton	50 mg·L^{-1}	Fe_3O_4/MWCNTs 2.9 g·L^{-1}	19.38 mmol/L	2	91.9	First order	—	—	[17]
Heterogeneous-Fenton	15 mg·L^{-1}	WO_3 2.44 mg·L^{-1}	0.179 mM·L^{-1}	4	92.8	First order			Our work
	60 mg·L^{-1}	WO_3 2.44 mg·L^{-1}	0.179 mM·L^{-1}		76.8	First order			

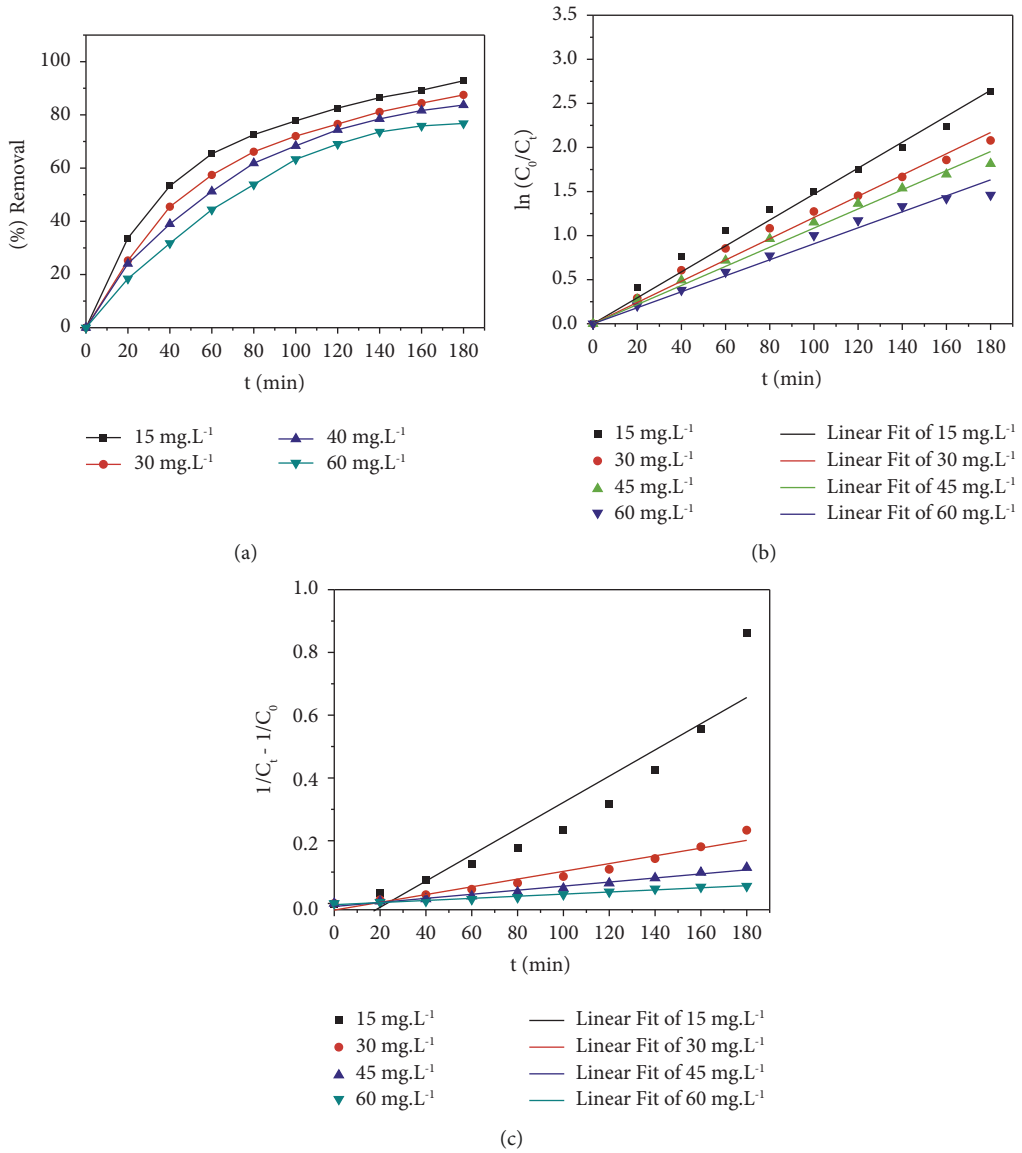

Figure 5: (a) Effect of initial concentration of MO on the degradation of methyl orange. (b) First- and (c) second-order kinetic model of the removal of MO. Experimental conditions: mass of WO3 = 0.25 g and pH = 4.

Table 2: Rate parameters of the removal of MO by WO_3/H_2O_2.

Initial concentration ($mg \cdot L^{-1}$)	Pseudo first-order model (min^{-1})		Pseudo second-order model $mol^{-1} \cdot L^{-1} \cdot min^{-1}$	
	$k_1 \times 10^{-2}$	R^2	$k_2 \times 10^{-3}$	R^2
15	1.42	0.996	1.16	0.879
30	1.19	0.995	0.58	0.953
45	1.03	0.996	0.31	0.977
60	0.88	0.994	2.99	0.983

order model based on regression coefficient values (R^2). The rate constants obtained from kinetic plots of the pseudo first-order model were higher than the pseudo second-order model.

The rate constant decreased from 0.0142 to 0.0088 min^{-1} with increase in concentration. The results indicated that the removal of lower concentrations of MO was faster than higher concentrations.

4. Conclusion

Kinetic models of the heterogeneous Fenton-like process were successfully studied in the degradation of MO. Tungsten oxide particles synthesized showed particles in nanosize and orthorhombic crystal structure. The couple WO_3/H_2O_2 was performed for the degradation of MO. The increase of the temperature of the reaction from 303 to 338 K showed the enhancement of the rate of MO removal. Temperature of 338 K showed the most effective degradation of MO with WO_3/H_2O_2. The rate of methyl orange removal increased with decreasing the

concentration of methyl orange. The kinetic studies indicated that the degradation of MO followed the first-order kinetics. Heterogeneous WO_3/H_2O_2 system can be a promising process for the treatment of dyes in wastewater.

Data Availability

Characterization and analytical data supporting the findings of this study are available from the corresponding author upon request. Table and figure data used to support the findings of this study are included within the article.

Conflicts of Interest

The authors declare that there are no conflicts of interest.

Acknowledgments

This work is supported by the Governmentof Cote d'Ivoire under the research program of merit PhD students. No funding was used in the study.

References

[1] M. Ikram, R. Asghar, M. Imran et al., "Experimental and computational study of Zr and CNC-doped MnO_2Nanorods for photocatalytic and antibacterial activity," *ACS Omega*, vol. 7, no. 16, pp. 14045–14056, 2022.

[2] M. Ikram, J. Hassan, A. Raza et al., "Photocatalytic and bactericidal properties and molecular docking analysis of TiO_2 nanoparticles conjugated with Zr for environmental remediation," *RSC Advances*, vol. 10, no. 50, pp. 30007–30024, 2020.

[3] M. Jamshaid, H. M. Khan, and M. A. Nazir, "A novel bentonite–cobalt doped bismuth ferrite nanoparticles with boosted visible light induced photodegradation of methyl orange: synthesis, characterization and analysis of physiochemical changes," *International Journal of Environmental Analytical Chemistry*, vol. 110, 2022.

[4] O. P. Kumar, M. Ahmad, M. A. Nazir et al., "Strategic combination of metal–organic frameworks and C3N4 for expeditious photocatalytic degradation of dye pollutants," *Environmental Science and Pollution Research*, vol. 29, no. 23, pp. 35300–35313, 2021.

[5] K. Shahzad, S. Hussain, M. Altaf Nazir et al., "Versatile Ag_2O and ZnO nanomaterials fabricated via annealed Ag-PMOS and ZnO-PMOS: an efficient photocatalysis tool for azo dyes," *Journal of Molecular Liquids*, vol. 356, Article ID 119036, 2022.

[6] K. Shahzad, T. Najam, M. S. Bashir et al., "Fabrication of periodic mesoporous organo silicate (PMOS) composites of Ag and ZnO: photo-catalytic degradation of methylene blue and methyl orange," *Inorganic Chemistry Communications*, vol. 123, Article ID 108357, 2021.

[7] H. Ghasemi, S. Mozaffari, S. H. Mousavi, B. Aghabarari, and N. Abu-Zahra, "Decolorization of wastewater by heterogeneous fenton reaction using MnO_2-Fe_3O_4/CuO hybrid catalysts," *Journal of Environmental Chemical Engineering*, vol. 9, no. 2, Article ID 105091, 2021.

[8] O. P. Kumar, K. Shahzad, M. A. Nazir et al., "Photo-Fenton activated C3N4x/AgOy@Co1-xBi0.1-yO7 dual s-scheme heterojunction towards degradation of organic pollutants," *Optical Materials*, vol. 126, Article ID 112199, 2022.

[9] J. P. Ribeiro and M. I. Nunes, "Recent trends and developments in fenton processes for industrial wastewater treatment–a critical review," *Environmental Research*, vol. 197, Article ID 110957, 2021.

[10] M. Zhang, Y. Niu, and Y. Xu, "Heterogeneous Fenton-like magnetic nanosphere coated with vanadium oxide quantum dots for enhanced organic dyes decolorization," *Journal of Colloid and Interface Science*, vol. 579, pp. 269–281, 2020.

[11] Y. Zhu, R. Zhu, Y. Xi, J. Zhu, G. Zhu, and H. He, "Strategies for enhancing the heterogeneous fenton catalytic reactivity: a review," *Applied Catalysis B: Environmental*, vol. 255, Article ID 117739, 2019.

[12] M. M. Bello, A. A. Abdul Raman, and A. Asghar, "A review on approaches for addressing the limitations of fenton oxidation for recalcitrant wastewater treatment," *Process Safety and Environmental Protection*, vol. 126, pp. 119–140, 2019.

[13] D. Wiedmer, E. Sagstuen, K. Welch, H. J. Haugen, and H. Tiainen, "Oxidative power of aqueous non-irradiated TiO_2-H_2O_2 suspensions: methylene blue degradation and the role of reactive oxygen species," *Applied Catalysis B: Environmental*, vol. 198, pp. 9–15, 2016.

[14] T. Rhadfi, J. Y. Piquemal, L. Sicard et al., "Polyol-made Mn_3O_4 nanocrystals as efficient fenton-like catalysts," *Applied Catalysis A: General*, vol. 386, no. 1-2, pp. 132–139, 2010.

[15] A. D. Bokare and W. Choi, "Review of iron-free Fenton-like systems for activating H_2O_2 in advanced oxidation processes," *Journal of Hazardous Materials*, vol. 275, pp. 121–135, 2014.

[16] A. M. G. Domacena, C. L. E. Aquino, and M. D. L. Balela, "Photo-Fenton degradation of methyl orange using hematite (α-Fe_2O_3) of various morphologies," *Materials Today Proceedings*, vol. 22, pp. 248–254, 2020.

[17] H. Y. Xu, Y. Wang, T. N. Shi et al., "Heterogeneous fenton-like discoloration of methyl orange using Fe3O4/MWCNTs as catalyst: kinetics and Fenton-like mechanism," *Frontiers of Materials Science*, vol. 12, no. 1, pp. 34–44, 2018.

[18] A. Omri, W. Hamza, and M. Benzina, "Photo-Fenton oxidation and mineralization of methyl orange using Fe-sand as effective heterogeneous catalyst," *Journal of Photochemistry and Photobiology A: Chemistry*, vol. 393, Article ID 112444, 2020.

[19] N. A. Youssef, S. A. Shaban, F. A. Ibrahim, and A. S. Mahmoud, "Degradation of methyl orange using fenton catalytic reaction," *Egyptian Journal of Petroleum*, vol. 25, no. 3, pp. 317–321, 2016.

[20] N. E. Séverin, S. E. Aimé, D. Donourou, B. O. Diby, and M. Y. Jocelin, "Catalytic activity of using tungsten oxide with hydrogen peroxide for methyl orange degradation," *African Journal of Pure and Applied Chemistry*, vol. 14, no. 4, pp. 69–80, 2020.

[21] S. N. gora. Eroi, A. S. Ello, D. Diabaté, and D. B. Ossonon, "Heterogeneous WO3/H2O2 system for degradation of indigo carmin dye from aqueous solution," *South African Journal of Chemical Engineering*, vol. 37, pp. 53–60, 2021.

[22] Y. Liu, Q. Li, S. Gao, and J. K. Shang, "Template-free solvothermal synthesis of WO3/WO 3·H2O hollow spheres and their enhanced photocatalytic activity from the mixture phase effect," *CrystEngComm*, vol. 16, no. 32, pp. 7493–7501, 2014.

[23] Y. Yu, W. Zeng, Z. Zhang, Y. Cai, and H. Zhang, "Hierarchical $WO3{\cdot}H_2O$ porous microsphere: hydrothermal synthesis, structure and gas-sensing performance," *Materials Letters*, vol. 186, pp. 119–122, 2017.

[24] S. Bae, S. Gim, H. Kim et al., "New features and uncovered benefits of polycrystalline magnetite as reusable catalyst in

reductive chemical conversion," *Journal of Physical Chemistry C*, vol. 121, no. 45, pp. 25195–25205, 2017.

[25] S. Bai, K. Zhang, L. Wang et al., "Synthesis mechanism and gas-sensing application of nanosheet-assembled tungsten oxide microspheres," *Journal of Materials Chemistry*, vol. 2, no. 21, pp. 7927–7934, 2014.

[26] S. Songara, V. Gupta, M. Kumar Patra et al., "Tuning of crystal phase structure in hydrated WO3 nanoparticles under wet chemical conditions and studies on their photochromic properties," *Journal of Physics and Chemistry of Solids*, vol. 73, no. 7, pp. 851–857, 2012.

[27] K. O. Iwu, A. Galeckas, P. Rauwel, A. Y. Kuznetsov, and T. Norby, "One-dimensional WO3 and its hydrate: one-step synthesis, structural and spectroscopic characterization," *Journal of Solid State Chemistry*, vol. 185, pp. 245–252, 2012.

[28] G. Jeevitha and D. Mangalaraj, "Ammonia sensing at ambient temperature using tungsten oxide (WO3) nanoparticles," *Materials Today Proceedings*, vol. 18, pp. 1602–1609, 2019.

[29] S. H. El-Khalafy, M. T. Hassanein, M. F. Abd-Elal, and A. A. Atia, "Oxidation of azo dye Orange II with hydrogen peroxide catalyzed by 5, 10, 15, 20-tetrakis (4-(diethylmethylammonio) phenyl) porphyrinato-cobalt (II) tetraiodide in aqueous solution," *Journal of Saudi Chemical Society*, vol. 24, no. 7, pp. 520–526, 2020.

[30] A. Kessler, J. Hedberg, E. Blomberg, and I. Odnevall, "Reactive oxygen species formed by metal and metal oxide nanoparticles in physiological media—a review of reactions of importance to nanotoxicity and proposal for categorization," *Nanomaterials*, vol. 12, 2022.

[31] P. Deka, A. Hazarika, R. C. Deka, and P. Bharali, "Influence of CuO morphology on the enhanced catalytic degradation of methylene blue and methyl orange," *RSC Advances*, vol. 6, no. 97, pp. 95292–95305, 2016.

[32] M. S. Osgouei, M. Khatamian, and H. Kakili, "Improved visible-light photocatalytic activity of Mn_3O_4-based nanocomposites in removal of methyl orange," *Materials Chemistry and Physics*, vol. 239, Article ID 122108, 2020.

[33] M. Ziolek and I. Sobczak, "The role of niobium component in heterogeneous catalysts," *Catalysis Today*, vol. 285, pp. 211–225, 2017.

[34] A. R. A. Giwa, I. A. Bello, A. B. Olabintan, O. S. Bello, and T. A. Saleh, "Kinetic and thermodynamic studies of fenton oxidative decolorization of methylene blue," *Heliyon*, vol. 6, no. 8, Article ID e04454, 2020.

[35] A. K. Hassan, G. Y. Al-Kindi, and D. Ghanim, "Green synthesis of bentonite-supported iron nanoparticles as a heterogeneous Fenton-like catalyst: kinetics of decolorization of reactive blue 238 dye," *Water Science and Engineering*, vol. 13, no. 4, pp. 286–298, 2020.

[36] M. Yuan, X. Fu, J. Yu et al., "Green synthesized iron nanoparticles as highly efficient fenton-like catalyst for degradation of dyes," *Chemosphere*, vol. 261, Article ID 127618, 2020.

[37] P. Mahamallik and A. Pal, "Photo-Fenton process in Co (II)-adsorbed admicellar soft-template on alumina support for methyl orange degradation," *Catalysis Today*, vol. 348, pp. 212–222, 2020.

[38] X. Duan, S. Indrawirawan, J. Kang et al., "Temperature-dependent evolution of hydroxyl radicals from peroxymonosulfate activation over nitrogen-modified carbon nanotubes," *Sustainable Materials and Technologies*, vol. 18, Article ID e00082, 2018.